

Protocol Dependence of the Jamming Transition

Thibault Bertrand,^{1,*} Robert P. Behringer,² Bulbul Chakraborty,³ Corey S. O'Hern,^{1,4,5} and Mark D. Shattuck^{6,1}

¹*Department of Mechanical Engineering and Materials Science,
Yale University, New Haven, Connecticut, 06520, USA*

²*Department of Physics and Center for Nonlinear and Complex Systems,
Duke University, Durham, North Carolina, 27708-0305, USA*

³*Martin Fisher School of Physics, Brandeis University,
Mail Stop 057, Waltham, Massachusetts, 02454-9110, USA*

⁴*Department of Physics, Yale University, New Haven, Connecticut, 06520, USA*

⁵*Department of Applied Physics, Yale University, New Haven, Connecticut, 06520, USA*

⁶*Department of Physics and Benjamin Levich Institute,
The City College of the City University of New York, New York, 10031, USA*

(Dated: March 5, 2022)

We propose a theoretical framework for predicting the protocol dependence of the jamming transition for frictionless spherical particles that interact via repulsive contact forces. We study isostatic jammed disk packings obtained via two protocols: isotropic compression and simple shear. We show that for frictionless systems, all jammed packings can be obtained via either protocol. However, the probability to obtain a particular jammed packing depends on the packing-generation protocol. We predict the average shear strain required to jam initially unjammed isotropically compressed packings from the density of jammed packings, shape of their basins of attraction, and path traversed in configuration space. We compare our predictions to simulations of shear strain-induced jamming and find quantitative agreement. We also show that the packing fraction range, over which shear strain-induced jamming occurs, tends to zero in the large system limit for frictionless packings with overdamped dynamics.

PACS numbers: 45.70.-n,61.43.-j,64.70.ps,83.80.Fg

I. INTRODUCTION

Dry granular materials are composed of macro-sized particles that interact via repulsive contact forces. Due to dissipative interactions between grains, granular materials exist as static packings in the absence of external driving [1]. As a consequence, granular packings are out-of-equilibrium, and their structural and mechanical properties depend on the protocol used to generate them. Experimental packing-generation protocols include gravitational deposition [2], vibration [3], compression [4], and shear [5, 6]. Several computational studies have pointed out that the distribution of jammed packing fractions depends on the compression rate [7, 8] and rate at which kinetic energy is removed from the system [9, 10]. In addition, experimental studies of photoelastic disks have identified key differences between granular packings generated via isotropic compression and pure shear [11].

There has been significant work on understanding the scaling behavior of the elastic moduli and contact number near jamming onset in model granular packings composed of frictionless spherical particles generated using isotropic compression [12]. However, there is currently no theoretical understanding of how the ensemble of static packings and their properties vary with the protocol used to generate them. For example, what is the difference in the distribution of jammed packings generated via

isotropic compression versus shear?

We focus on isostatic jammed packings of frictionless disks generated via different combinations of isotropic compression and simple shear and study the distribution of jammed packings as a function of the path taken through configuration space. A recent study has distinguished between ‘compression-only’ jammed packings that possess non-zero pressure and positive shear moduli for some but not all boundary deformations, and ‘shear-stabilized’ jammed packings that possess positive shear moduli for all shear deformations [13]. We describe the protocol dependence of *compression-only* jammed packings, which are experimentally realizable [14] and are relevant for understanding jamming in systems with frictional interactions [15].

We find several important results. First, an exponentially large but finite number of jammed packings with an isostatic number of contacts $N_c = N_c^{\text{iso}} = 2N' - 1$ (where N' is the number of disks in the force-bearing backbone) exist in configuration space, defined by the disk positions, packing fraction ϕ , and shear strain deformation γ of the system boundaries. In small systems, nearly all jammed packings can be enumerated [14]. For example, we have shown that isostatic jammed packings form one-dimensional geometrical families as a function of shear strain [16]. We will show that the choice of the packing-generation protocol does not change the ensemble of isostatic, jammed packings, but instead changes which packings are visited during particular trajectories through configuration space. The average properties of jammed packings change for different protocols be-

*Electronic address: thibault.bertrand@yale.edu

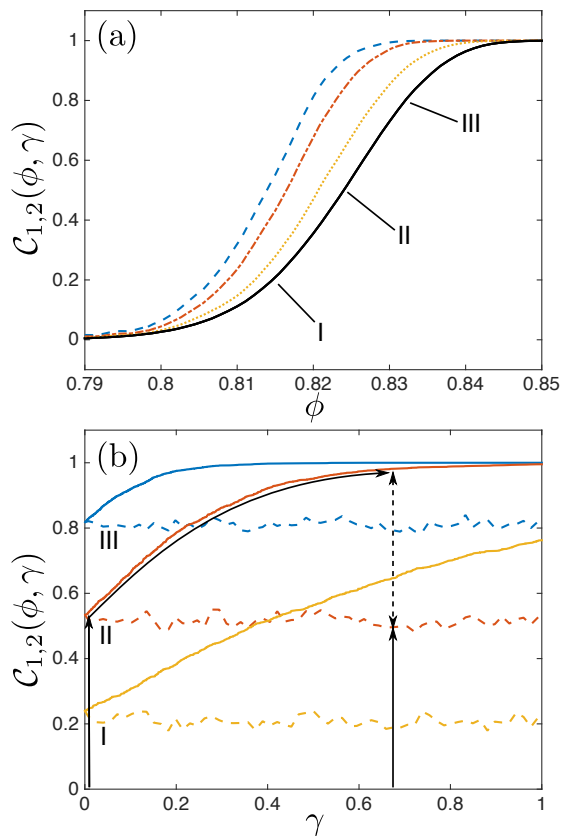


FIG. 1: Fraction of jammed packings (or cumulative distribution) $\mathcal{C}(\phi, \gamma)$ along different paths in the packing fraction ϕ and shear strain γ plane for $N = 32$. (a) $\mathcal{C}_1(\phi, \gamma)$ for protocol 1 (isotropic compression at fixed γ ; solid line) and $\mathcal{C}_2(\phi, \gamma)$ for protocol 2, *i.e.* compression to ϕ followed by shear strain to $\gamma = 0.1$ (dotted line), 0.3 (dot-dashed line), and 0.5 (dashed line). I, II, and III indicate the packing fractions in (b). (b) We show $\mathcal{C}_1(\phi, \gamma)$ (dashed lines) and $\mathcal{C}_2(\phi, \gamma)$ (solid lines) at fixed $\phi = 0.815, 0.824, \text{ and } 0.832$ indicated by I-III. Protocol dependence can be seen in the difference between \mathcal{C}_1 and \mathcal{C}_2 evaluated at the same ϕ and γ , *e.g.* at $\phi = 0.824$ and $\gamma = 0.67$ as highlighted by the dashed double arrow. Right and left solid arrows indicate protocols 1 and 2, respectively.

cause the probabilities for obtaining each jammed packing varies with protocol.

We develop a theoretical description of the protocol dependence of the distribution of jammed disk packings (Fig. 1). We assume that an initially unjammed system will jam when it encounters the basin of attraction of a jammed packing as it travels through configuration space. The probability to obtain a jammed packing is determined by two factors: 1) the number density of jammed packings in configuration space, which is independent of the packing protocol, and 2) the path traveled through configuration space, which depends on the protocol. Using this framework, we predict the average shear strain to jam initially unjammed packings at each ϕ and show that the predictions agree with simulations of shear strain-

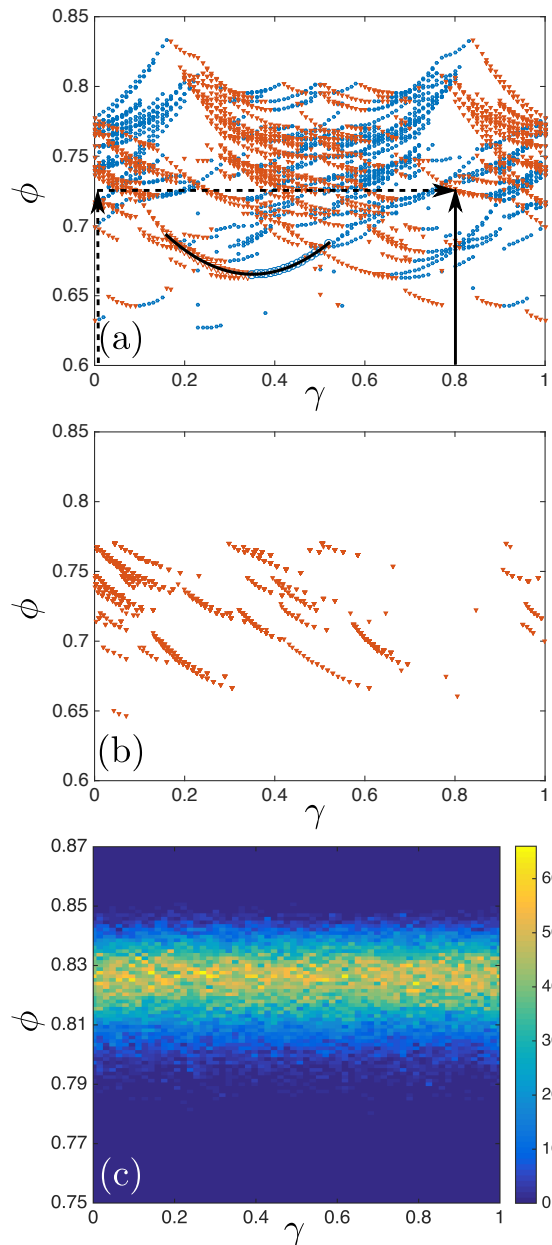


FIG. 2: (a) Packing fraction ϕ versus shear strain γ for all isostatic jammed $N = 6$ disk packings. The solid black line obeys $\phi = A(\gamma - \gamma_0)^2 + \phi_0$ with $A = 0.776$, $\phi_0 = 0.665$, and $\gamma_0 = 0.35$. Filled circles (downward triangles) indicate packings with positive (negative) local slope. The solid vertical arrow indicates protocol 1, and the dashed vertical arrow followed by the dashed horizontal arrow indicates protocol 2 that was used to reach a jammed packing at $\gamma = 0.8$ and $\phi = 0.725$. (b) Jammed packing fraction $\phi(\gamma)$ using protocol 2 at fixed ϕ in the range $0.64 < \phi < 0.77$ for $N = 6$. (c) Number of $N = 32$ jammed packings at each ϕ and γ (increasing from dark to light) from protocol 1.

induced jamming. Our results indicate that the packing fraction range, over which shear strain-induced jamming occurs, vanishes in the large-system limit for overdamped

frictionless systems.

The remainder of the manuscript is organized into three sections. In Sec. II, we describe our simulation methods and introduce the two protocols used to generate isostatic jammed packings. In Sec. III, we show results concerning the protocol dependence of the distribution of jammed packings. We then describe a theoretical model that allows us to calculate the probability to obtain jammed packings as a function of the path that the system traverses in configuration space. In Sec. IV, we summarize our results and conclusions.

II. METHODS

We study systems containing N frictionless bidisperse disks in a parallelogram with height $L = 1$ in two dimensions (2D) that interact via purely repulsive linear spring forces with energy scale ϵ [17]. (Studies of bidisperse frictionless spheres in three dimensions are included in Appendix A.) The mixtures contain half large and half small particles with mass $m = 1$ for both and diameter ratio $\sigma_L/\sigma_S = 1.4$. We employ Lees-Edwards simple shear-periodic boundary conditions, where the top (bottom) images of the central cell are shifted to the right (left) by $\pm\gamma L$ and γ is the shear strain [18]. We varied the system size from $N = 6$ to 512 particles.

Below, we describe results for two protocols to generate jammed packings in the ϕ - γ plane. (See Fig. 2 (a).) Protocol 1 involves isotropic compression at fixed boundary shape parametrized by shear strain γ . We start with random initial disk positions at $\phi_0 < 0.5$. We successively compress the system by increasing particle radii uniformly in small packing fraction increments $d\phi$ and minimize the total potential energy per particle $V/(N\epsilon)$ (at fixed γ) after each step. Jamming onset occurs when $V_{\max} > V/(N\epsilon) > 0$, with $V_{\max} = 10^{-16}$, or an equivalent threshold on pressure. For protocol 2, we start by isotropically compressing systems (at $\gamma = 0$) to ϕ , and if the system is unjammed with $V/(N\epsilon) \ll V_{\max}$, we successively apply simple shear strain to each particle $x'_i = x_i + d\gamma y_i$ in strain steps $d\gamma < 10^{-3}$ followed by minimization of $V/(N\epsilon)$. We then identify the total shear strain γ at which the system first jams with $10^{-16} > V/(N\epsilon) > 0$. Protocols 1 and 2 generate compression-only jammed packings. In Appendix C, we also describe results for a third protocol, which is similar to protocol 2, but with simple shear replaced by pure shear. Note that isostatic jammed packings can also be generated using stress-controlled packing-generation protocols [21].

III. RESULTS

We display the cumulative distributions $\mathcal{C}_{1,2}(\phi, \gamma)$ of jammed packings from protocols 1 and 2 in Fig. 1. In (a), we show that applying shear strain increases the fraction

of jammed packings at each ϕ , *i.e.* $\mathcal{C}_2(\gamma, \phi)$ shifts to lower ϕ with increasing γ . In (b), we show $\mathcal{C}_1(\phi, \gamma)$ obtained via isotropic compression versus boundary shape for $\phi = 0.815, 0.824, \text{ and } 0.832$ (corresponding to $\mathcal{C}_1(\phi, 0) \approx 0.2, 0.5, \text{ and } 0.8$). $1 - \mathcal{C}_1(\phi, 0)$ of the packings are initially unjammed at $\gamma = 0$ and ϕ , and these jam with increasing γ as shown by the solid lines. By combining different amounts of shear strain and isotropic compression, the fraction of jammed packings at a given ϕ can be tuned over a wide range, *e.g.* from 0.2 to 0.8 for packings at $\phi = 0.815$. These results emphasize that the distribution of jammed packings depends strongly on the path through configuration space, *e.g.* protocols 1 and 2 indicated by the arrows in Fig. 1 (b).

To understand protocol dependence, we examine the distribution of jammed packings in the ϕ - γ plane. In Fig. 2 (a), we show the packing fraction at jamming onset ϕ versus γ for $N = 6$ from protocol 1 (solid vertical arrow in Fig. 2 (a)). We find several striking features. First, jammed packings occur as geometrical families (*i.e.* segments of parabolas that correspond to jammed packings with the same interparticle contact network) in the ϕ - γ plane. For $N = 6$, we are able to enumerate nearly all geometrical families over the full range of γ [16]. When straining an initially unjammed system toward positive γ at fixed ϕ (*e.g.* horizontal arrow in Fig. 2 (a)), it will jam on a geometrical family with negative slope ($-|d\phi/d\gamma|$). For negative slopes, continued shear strain leads to overcompression, whereas for positive slopes, continued shear strain leads to unjamming. This behavior is shown in Fig. 2 (b) for protocol 2 at fixed ϕ in the range $0.64 < \phi < 0.77$ for $N = 6$. Note that any of the jammed packings in Fig. 2 (b) from protocol 2 and defined by $\{\vec{r}_i\}$, ϕ , and γ can be generated using protocol 1 with initial condition $\{\vec{r}_i\}$ and boundary deformation γ . As a result, we can generate the same jammed packing at a given ϕ and γ using different combinations of compression and shear strain. We find similar behavior to that in Fig. 2 (a) and (b) for larger N , except that the parabolic segments in $\phi(\gamma)$ become smaller and more numerous, and thus geometrical families more densely populate configuration space (Fig. 2 (c)). The number of jammed packings (at a given ϕ and γ) becomes independent of γ for $N \geq 32$.

We develop a theoretical model using an analogy with absorption problems to calculate the probability to obtain isostatic jammed packings as a function of the path that the system traverses in configuration space. In principle, the number density of jammed packings \mathcal{F} depends on the $2N$ coordinates of the disks, ϕ , and γ , but not the packing-generation protocol. After integrating over the $2N$ disk coordinates, \mathcal{F} is a function of ϕ and γ . However, we assume that the number density $\mathcal{F}(\phi)$ is only a function of ϕ since \mathcal{F} becomes independent of γ in the large- N limit (Fig. 3 (c)). We imagine that a one-dimensional trajectory $\mathcal{L}(\phi, \gamma)$ through configuration space will encounter the basin of attraction [19] of a jammed packing with a probability $\mathcal{F}(\phi)S(\phi)d\mathcal{L}$ during a step of size

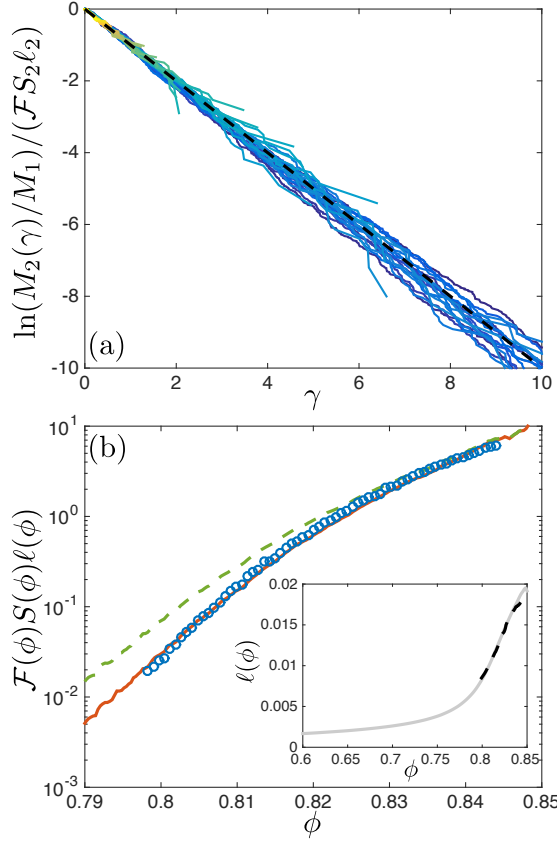


FIG. 3: (a) Natural logarithm of the fraction of unjammed packings (normalized by the ϕ -dependent decay factor, $\mathcal{F}(\phi)S_2(\phi)\ell_2(\phi)$), during protocol 2 at fixed ϕ in the range $0.798 < \phi < 0.844$ (solid lines) for $N = 32$. The dashed line has slope -1 . (b) Comparison of $-d\ln[M_2(\phi, \gamma)/M_0]/d\gamma$ (open circles) from protocol 2 and $-d\ln[M_1(\phi)/M_0]/d\phi$ from protocol 1 with $S_2(\phi) \propto S_1(\phi)\ell_1(\phi)$ (solid line) or $S_2(\phi) \propto S_1(\phi)$ (dashed line) for $N = 32$. The inset shows the distances $\ell_1(\phi)$ and $\alpha\ell_2(\phi)$ (with $\alpha \approx 5.5$) traversed in configuration space during protocols 1 (solid line) and 2 (dashed line) for $N = 32$.

$d\mathcal{L}$ in configuration space, where $S(\phi)$ is the $2N - 1$ -dimensional cross-section of the basin of attraction of a jammed packing perpendicular to $d\mathcal{L}$.

Thus, for protocol 1 with trajectories only along ϕ , the decrease in the number of unjammed packings $dM_1(\phi)$ (or equivalently, increase in the number of jammed packings) during a compression step $d\phi$ is

$$dM_1(\phi) = -M_1(\phi)\mathcal{F}(\phi)S_1(\phi)\ell_1(\phi)d\phi, \quad (1)$$

where $d\mathcal{L} = \ell_1(\phi)d\phi$, $\ell_1(\phi)$ is the distance in configuration space traversed during step $d\phi$ at ϕ , and $S_1(\phi)$ is the average cross section for protocol 1. Eq. 1 can be solved for the number of unjammed packings at ϕ during protocol 1:

$$M_1(\phi) = M_0 \exp \left[- \int_{\phi_0}^{\phi} \mathcal{F}(\phi')S_1(\phi')\ell_1(\phi')d\phi' \right], \quad (2)$$

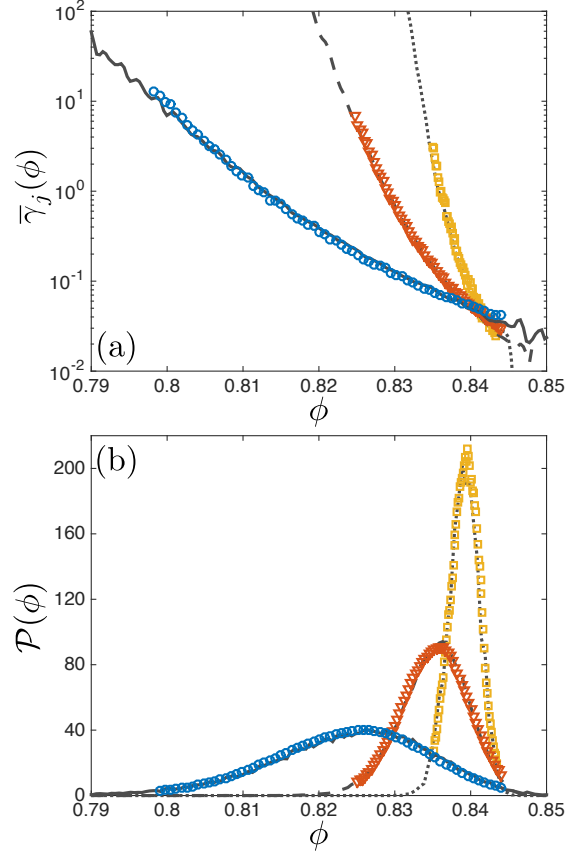


FIG. 4: (a) Average shear strain $\bar{\gamma}_j(\phi)$ to jam an initially unjammed configuration at ϕ and $\gamma = 0$ (protocol 2) for $N = 32$ (circles), 128 (triangles), and 512 (squares). We compare $\bar{\gamma}_j(\phi)$ from protocol 2 to $1/(\mathcal{F}(\phi)S_1(\phi)\ell_1^2(\phi))$ (Eqs. 3 and 4) from protocol 1 for the same system sizes: $N = 32$ (solid line), 128 (dashed line), and 512 (dotted line). (b) Distribution of jammed packing fractions $\mathcal{P}_1(\phi)$ from protocol 1 for $N = 32$ (solid line), 128 (dashed line), and 512 (dotted line) compared to predictions obtained from $\mathcal{P}_1(\phi) = -M_0^{-1}dM_1(\phi)/d\phi$ with $M_1(\phi)$ given by Eq. 2 and $\mathcal{F}(\phi)S_1(\phi)\ell_1(\phi)$ given by Eq. 4 using the measured value of $\bar{\gamma}_j$ for $N = 32$ (circles), 128 (triangles), and 512 (squares).

where M_0 is the number of unjammed packings at ϕ_0 . For protocol 2, with trajectories only along γ , we obtain a similar expression for the number of unjammed packings: $dM_2(\phi, \gamma)/d\gamma = -M_2(\phi, \gamma)\mathcal{F}(\phi)S_2(\phi)\ell_2(\phi)$, where $M_2(\phi, \gamma) = M_1(\phi)\exp[-\mathcal{F}(\phi)S_2(\phi)\ell_2(\phi)\gamma]$, $S_2(\phi)$ is the average cross section for protocol 2, and $\ell_2(\phi)$ is the distance traversed in configuration space for each shear strain step $d\gamma$.

Fig. 3 (a) shows that the fraction of unjammed packings $M_2(\phi, \gamma)/M_1(\phi)$ decays exponentially with γ during protocol 2 at each ϕ . This result emphasizes that we can calculate the product $\mathcal{F}(\phi)S(\phi)\ell(\phi)$ without enumeration of all jammed packings by measuring the decrease in the number of jammed packings with increasing shear strain. In the zeroth order approximation, the cross section $S(\phi)$ is independent of the path in configuration space and the

distance ℓ traveled during each $d\phi$ or $d\gamma$ step is constant. In Fig. 3 (b), we compare $\mathcal{F}(\phi)S(\phi)\ell$ from protocol 2 with the similar quantity $-d\ln[M_1(\phi)/M_0]/d\phi$ from protocol 1 and find qualitative agreement.

We then independently measured $\ell_1(\phi)$, defined by the accumulated distance in configuration space between the initial packing at ϕ and relaxed packing at $\phi + d\phi$, for protocol 1. We performed similar measurements for $\ell_2(\phi)$, which gives the accumulated distance in configuration space between the initial packing at γ and relaxed packing at $\gamma + d\gamma$ for protocol 2. We show that the two are proportional to each other, $\ell_1(\phi) = \alpha\ell_2(\phi)$ with $\alpha \approx 5.5$, in the inset of Fig. 3 (b). By calculating $-d\ln[M_1(\phi)/M_0]/d\phi = \mathcal{F}(\phi)S_1(\phi)\ell_1(\phi)$ for protocol 1, we can compare $\mathcal{F}(\phi)S_1(\phi)\ell_1(\phi)$ to the similar quantity, $\mathcal{F}(\phi)S_2(\phi)\ell_2(\phi)$, for protocol 2. In this case, we assume that the cross section depends on the path in configuration space, *e.g.* isotropic compression increases the overlaps of all interparticle contacts, while shear strain increases some but decreases others. In Fig. 3 (b), we show excellent agreement for $\mathcal{F}(\phi)S_{1,2}(\phi)\ell_{1,2}(\phi)$ for protocols 1 and 2 for $N = 32$ provided we assume that $S_2(\phi) \propto S_1(\phi)\ell_1(\phi)$, and find similar quantitative agreement for all system sizes studied. (Additional details of the theoretical model are included in Appendix D.) Independent measurements of $S_{1,2}(\phi)$ will be performed in future studies.

We now use the theoretical description of the protocol-dependent probability to jam to predict the average shear strain required to jam an initially unjammed isotropically compressed configuration at ϕ and $\gamma = 0$:

$$\begin{aligned} \bar{\gamma}_j(\phi) &= \int_0^\infty \gamma \frac{M_2(\phi, \gamma)}{M_1(\phi)} d\gamma = \frac{1}{\mathcal{F}(\phi)S_2(\phi)\ell_2(\phi)} \quad (3) \\ &\simeq \frac{\alpha}{\mathcal{F}(\phi)S_1(\phi)\ell_1^2(\phi)}. \quad (4) \end{aligned}$$

In Fig. 4 (a), we show that the prediction for $\bar{\gamma}_j(\phi)$, obtained from measurements of $\mathcal{F}(\phi)S_1(\phi)\ell_1^2(\phi)$ using isotropic compression, agrees with simulations of shear strain-induced jamming. We find that $\bar{\gamma}_j$ grows rapidly with increasing system size and only packings with $\phi \gtrsim 0.84$ are jammed in the large-system limit [20]. (We find similar results for applied pure shear in Appendix C.) We also calculate the distribution $\mathcal{P}_1(\phi)$ of jammed packing fractions (for isotropic compression) using data from protocol 2. In Fig. 4 (b), we show that $\mathcal{P}_1(\phi)$ from protocol 1 and $\mathcal{P}_1(\phi) = -M_0^{-1}dM_1(\phi)/d\phi$ with $M_1(\phi)$ given by Eq. 2 and $\mathcal{F}(\phi)S_1(\phi)\ell_1(\phi)$ given by Eq. 4 (using the measured value of $\bar{\gamma}_j$) collapse for all system sizes studied. The width of $\mathcal{P}_1(\phi)$ for isotropic compression narrows as $1/N^\lambda$ with $\lambda \approx 0.55 \pm 0.05$ and the peak approaches $\phi_{\text{rcp}} \approx 0.84$ in the large-system limit [20].

IV. CONCLUSION

In this manuscript, we developed a theoretical description for jamming onset that allows us to predict the

fraction of isostatic jammed packings that occur at ϕ and γ in terms of the path traversed in configuration space. This framework provides predictions for the average shear-strain required to jam initially unjammed packings produced by isotropic compression, which agree quantitatively with simulations of strain-induced jamming in two- and three-dimensional systems subjected to simple and pure shear. In particular, we showed that the packing fraction range, over which strain-induced jamming occurs, shrinks to zero in the large-system limit for frictionless systems with overdamped dynamics. In future studies, we will investigate the role of static friction in stabilizing strain-induced jamming of dilute granular packings [5].

Acknowledgments

We acknowledge support from the W. M. Keck Foundation Grant No. DT061314 (T.B., R.B., B.C., and C.S.O.), and National Science Foundation (NSF) Grant Nos. CBET-0968013 (M.D.S.) and DMR-1409093 (B.C.). We also acknowledge support from the Kavli Institute for Theoretical Physics (NSF Grant No. PHY-1125915), where some of this work was performed. This work benefited from the facilities and staff of the Yale University Faculty of Arts and Sciences High Performance Computing Center and NSF Grant No. CNS-0821132 that in part funded acquisition of the computational facilities.

Appendix A: 3D bidisperse packings

In this section, we present our studies of compression and shear-strain induced jamming of 3D bidisperse spheres, which are qualitatively similar to the results for 2D bidisperse systems presented in the main text. We presented results in the main text on the distribution of jammed packing fractions $\mathcal{P}(\phi)$ and average shear strain $\bar{\gamma}_j$ required to induce jamming in an originally unjammed configuration for systems composed of bidisperse disks in two spatial dimensions ($d = 2$). However, these results apply more generally than simply to two-dimensional packings of disks. The theoretical analysis in the main text described trajectories in the dN -dimensional configuration space in which jammed packings exist, where d is the spatial dimension. The $2N$ -dimensional configuration space is already large, and thus we expect qualitatively the same results for three-dimensional (3D) sphere packings, which exist in a configuration space that is only 50% larger, as we found for two-dimensional systems.

We studied systems containing N frictionless bidisperse spheres in a parallelepiped with sides of length $L = 1$ that interact via purely repulsive linear spring forces. The bidisperse mixtures contain half large and half small particles, both with mass $m = 1$, and diameter ratio $\sigma_L/\sigma_S = 1.4$. As in 2D, we employ Lees-Edwards

simple shear-periodic boundary conditions, where the top (bottom) images of the central cell are shifted to the right (left) by γL , where γ is the simple shear strain.

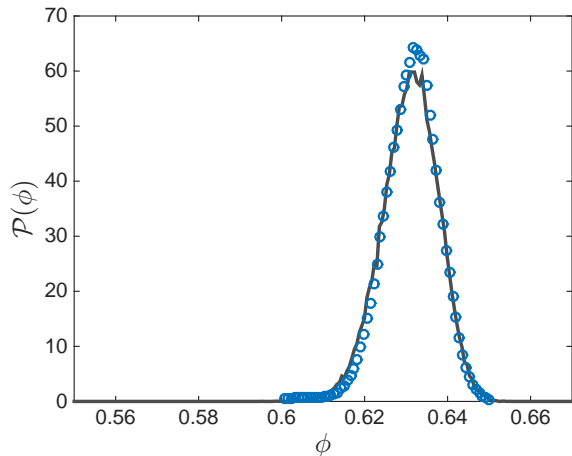


FIG. 5: Distribution of jammed packing fractions $\mathcal{P}_1(\phi)$ from protocol 1 for $N = 64$ bidisperse spheres (solid line), compared to predictions obtained from $\mathcal{P}_1(\phi) = -M_0^{-1}dM_1(\phi)/d\phi$ with $M_1(\phi)$ given by Eq. 2 and $\mathcal{F}(\phi)S_1(\phi)l_1(\phi)$ given by Eq. 4 using the measured value of $\bar{\gamma}_j$ for $N = 64$ bidisperse spheres (circles).

Here, we confirm that we can calculate the distribution $\mathcal{P}_1(\phi)$ of jammed packing fractions (for isotropic compression) using data from protocol 2. In Fig. 5, we show that $\mathcal{P}_1(\phi)$ from protocol 1 agrees with $\mathcal{P}_1(\phi) = -M_0^{-1}dM_1(\phi)/d\phi$ with

$$M_1(\phi) = M_0 \exp \left[- \int_{\phi_0}^{\phi} \mathcal{F}(\phi') S_1(\phi') l_1(\phi') d\phi' \right], \quad (\text{A1})$$

and the product $\mathcal{F}S_1l_1$ given by the measured value of $\bar{\gamma}_j$,

$$\bar{\gamma}_j(\phi) \simeq \frac{\alpha}{\mathcal{F}(\phi)S_1(\phi)l_1^\beta(\phi)}. \quad (\text{A2})$$

We find that $\beta \approx 1.75$ in 3D, whereas $\beta \approx 2.0$ in 2D.

Appendix B: Stress anisotropy in frictionless packings

In this Appendix, we show the typical structure of the geometrical families for frictionless packings and measure the ratio of the stress anisotropy to the pressure for these packings. When deforming granular packings, the deformation method can be either strain- or stress-controlled. In strain-controlled deformations, a strain is applied to the system and the resulting stress is measured. In contrast, in stress-controlled deformations, a stress is applied to the system, and the resulting strain is measured. In simulations with periodic boundary conditions, one

of the simplest deformation methods is the application of simple shear strain γ using Lees-Edwards boundary conditions. Thus, Lees-Edwards simple shear is strain-controlled. During the applied simple shear strain, one can measure the resulting stress of the system.

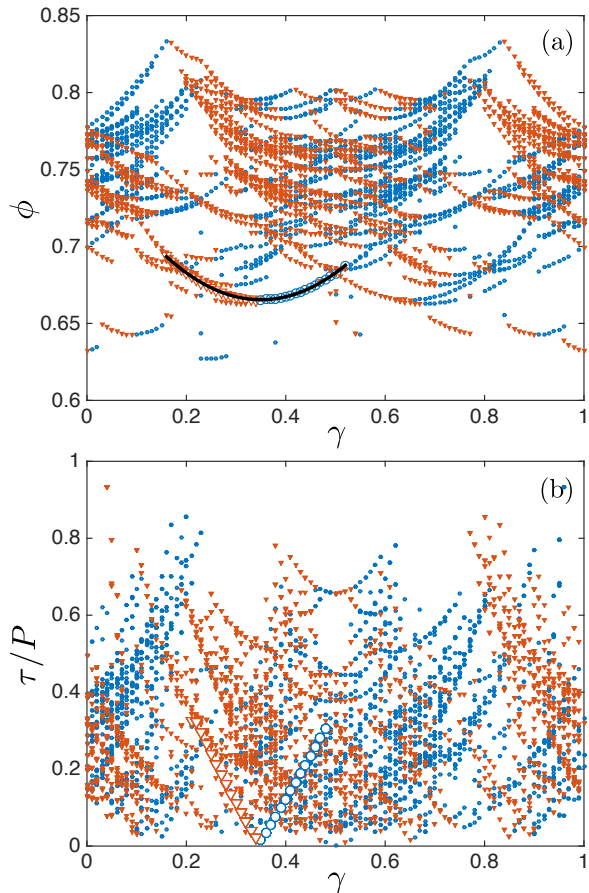


FIG. 6: (a) Packing fraction ϕ and (b) ratio of the stress anisotropy τ to the pressure P versus shear strain γ for all isotatic jammed $N = 6$ bidisperse disk packings. The solid black line in (a) obeys $\phi = A(\gamma - \gamma_0)^2 + \phi_0$ with $A = 0.776$, $\phi_0 = 0.665$, and $\gamma_0 = 0.35$. Filled circles (downward triangles) indicate packings with positive (negative) local slope of ϕ versus γ .

To measure the stress in 2D, we define the 2×2 stress tensor

$$\Sigma_{\lambda\delta} = \frac{1}{L^2} \sum_{i>j} f_{ij\lambda} r_{ij\delta}, \quad (\text{B1})$$

where $f_{ij\lambda}$ is the λ -component of the pairwise repulsive force \vec{f}_{ij} on particle i from particle j , $r_{ij\delta}$ is the δ -component of the center-to-center distance vector \vec{r}_{ij} between particles i and j , $\lambda = x, y$, and $\delta = x, y$. In Fig. 6 (b), we show the ratio of the stress anisotropy $\tau = |\Sigma_1 - \Sigma_2|/2$ to the pressure $P = (\Sigma_1 + \Sigma_2)/2$, where Σ_1 and Σ_2 are the two eigenvalues of the stress tensor, as a function of the shear strain γ . In many cases the

normalized stress anisotropy τ/P follows nearly linear segments along the geometrical families, which appear as parabolas when ϕ for each jammed packing is plotted versus γ (Fig. 6 (a)). However, for other geometrical families, τ/P appears quadratic in γ . For both cases, τ/P decreases when $-|d\phi/d\gamma| \leq 0$ and increases when $d\phi/d\gamma \geq 0$ along each geometrical family.

Appendix C: Comparison of pure and simple shear

In this Appendix, we compare results for simple shear and pure shear protocols. All of the results for protocol 2 presented in the main text were obtained using simple shear strain using Lees-Edwards boundary conditions. We have also studied strain-induced jamming using pure shear, where the separation between one pair of opposing edges of the simulation box is increased by $1 + \gamma$ and the separation between the other pair of opposing edges is decreased by $1/(1 + \gamma)$. This deformation is the simplest example of a variable-shape simulation cell method that conserves volume.

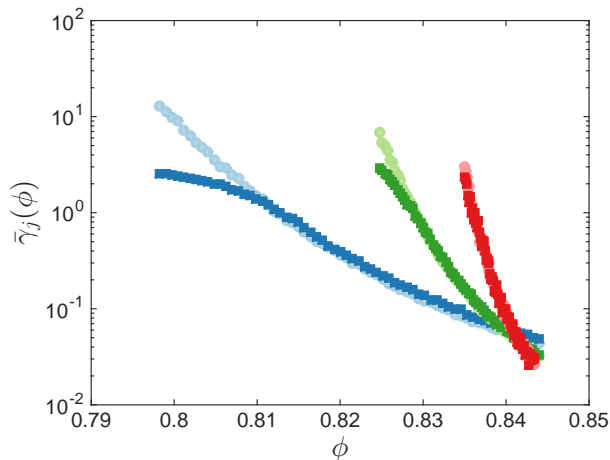


FIG. 7: Average shear strain $\bar{\gamma}_j(\phi)$ required to jam an initially unjammed configuration at ϕ using simple shear (light circles) and pure shear strain (dark squares) for $N = 32$ (blue symbols), 128 (green symbols), and 512 (red symbols).

We show in Fig. 7 that the strain $\bar{\gamma}_j(\phi)$ required to jam an initially unjammed configuration at packing fraction ϕ behaves qualitatively the same for packings generated via simple and pure shear strain. We see that the results for $\bar{\gamma}_j$ for simple and pure shear strain begin to deviate at low ϕ , but the deviation decreases with increasing system size. In the studies of pure shear, we stopped the simulations when the size of the cell in the thin direction caused interactions between a disk in the main cell and one of its own periodic images. If the system had not yet jammed, we did not include this trial in the measurement

of $\bar{\gamma}_j$. Thus, in the pure shear simulations, our results at low ϕ and small system sizes were biased toward small strains. This effect vanishes in the large-system limit.

Appendix D: Theoretical model

In this Appendix, we elaborate some of the key aspects of the theoretical model described in the main text. We develop the theoretical model using an analogy with absorption problems to calculate the probability to obtain isostatic jammed packings as a function of the path that the system traverses in configuration space. In principle, the number density of jammed packings \mathcal{F} , depends on the $2N$ coordinates of the disks, the packing fraction ϕ , and boundary deformation γ , but not the packing-generation protocol. After integrating over the $2N$ coordinates of the disks, \mathcal{F} is a function of ϕ and γ . However, for the theoretical description, we assume that the number density $\mathcal{F}(\phi)$ is only a function of packing fraction since \mathcal{F} becomes independent of γ in the large system limit as shown in Fig. 2 (c) in the main text.

We imagine that a one-dimensional trajectory $\mathcal{L}(\phi, \gamma)$ through configuration space will encounter the basin of attraction of a jammed packing with a probability $\mathcal{F}(\phi)S(\phi)d\mathcal{L}$ during a step of size $d\mathcal{L}$ in configuration space, where $S(\phi)$ is the $2N - 1$ -dimensional cross-section of the basin of attraction of a jammed packing perpendicular to $d\mathcal{L}$ and $d\mathcal{L} = \ell_1(\phi)d\phi$ and $\ell_2(\phi)d\gamma$ for protocols 1 and 2, respectively.

For the results presented in this manuscript, our calculations do not require complete enumeration of jammed packings and independent measurements of $\mathcal{F}(\phi)$, $S(\phi)$, and $\ell(\phi)$. An advantage of our work is that we showed that one can obtain the product $\mathcal{F}S\ell$ without complete enumeration by measuring the decrease in the number of unjammed configurations during shear. We showed (for fast quenching protocols) that the product $\mathcal{F}S\ell$ depends only on the packing fraction ϕ , and not on the shear strain γ . This result implies that we can use the shear protocol to predict the distribution of jammed packings obtained from the isotropic compression protocol.

To obtain $\ell_{1,2}$, we measured the cumulative distance traveled by the system in configuration space after taking a step in packing fraction $d\phi$ (Protocol 1) or a step in shear strain $d\gamma$ (Protocol 2) and minimizing the total potential energy:

$$\ell_{1,2}(\phi) = \sqrt{\sum_{i=1}^N |\delta \vec{r}_i|^2}, \quad (\text{D1})$$

where $\delta \vec{r}_i$ is the change in position of particle i following the compression or shear step and subsequent energy minimization. We averaged $\ell_{1,2}(\phi)$ over at least 100 independent trajectories.

-
- [1] H. M. Jaeger, S. R. Nagel, and R. P. Behringer, *Rev. Mod. Phys.* **68** (1996) 1259.
- [2] G. Y. Onoda and E. G. Liniger, *Phys. Rev. Lett.* **64** (1990) 2727.
- [3] E. R. Nowak, J. B. Knight, E. Ben-Naim, H. M. Jaeger, and S. R. Nagel, *Phys. Rev. E* **57** (1998) 1971.
- [4] T. S. Majmudar, M. Sperl, S. Luding, and R. P. Behringer, *Phys. Rev. Lett.* **98** (2007) 058001.
- [5] D. Bi, J. Zhang, B. Chakraborty, and R. P. Behringer, *Nature* **480** (2011) 355.
- [6] N. Kumar and S. Luding, arXiv:1407.6167.
- [7] S. Torquato, T. M. Truskett, and P. G. Debenedetti, *Phys. Rev. Lett.* **84** (2000) 2064.
- [8] K. Zhang, W. W. Smith, M. Wang, Y. Liu, J. Schroers, M. D. Shattuck, and C. S. O'Hern, *Phys. Rev. E* **90** (2014) 032311.
- [9] P. Chaudhuri, L. Berthier, and S. Sastry, *Phys. Rev. Lett.* **104** (2010) 165701.
- [10] C. F. Schreck, C. S. O'Hern, and L. E. Silbert, *Phys. Rev. E* **84** (2011) 011305.
- [11] T. S. Majmudar and R. P. Behringer, *Nature* **435** (2005) 1079.
- [12] A. J. Liu and S. R. Nagel, *Ann. Rev. Condens. Matter Phys.* **1** (2010) 347.
- [13] S. Dagois-Bohy, B. P. Tighe, J. Simon, S. Henkes, and M. van Hecke, *Phys. Rev. Lett.* **109** (2012) 095703.
- [14] G.-J. Gao, J. Blawdziewicz, C. S. O'Hern, and M. D. Shattuck, *Phys. Rev. E* **80** (2009) 061304.
- [15] T. Shen, S. Papanikolaou, C. S. O'Hern, and M. D. Shattuck, *Phys. Rev. Lett.* **113** (2014) 128302.
- [16] G.-J. Gao, J. Blawdziewicz, and C. S. O'Hern, *Phys. Rev. E* **80** (2009) 061303.
- [17] C. S. O'Hern, L. E. Silbert, A. J. Liu, and S. R. Nagel, *Phys. Rev. E* **68** (2003) 011306.
- [18] A. W. Lees and S. F. Edwards, *J. Phys. C Solid State* **5** (1972) 1921.
- [19] S. S. Ashwin, J. Blawdziewicz, C. S. O'Hern, and M. D. Shattuck, *Phys. Rev. E* **85** (2012) 061307.
- [20] N. Xu, J. Blawdziewicz, and C. S. O'Hern, *Phys. Rev. E* **71** (2005) 061306.
- [21] K. C. Smith, I. Srivastava, T. S. Fisher, and M. Alam, *Phys. Rev. E* **89** (2014) 042203.